16th INTERNATIONAL POWER ELECTRONICS AND MOTION CONTROL CONFERENCE AND EXPOSITION (PEMC 2014)

ORGANIZERS

SPONSORS

SUPPORTERS

Antalya-TURKEY
21-24 September 2014
http://www.pemc2014.org

CATALOG NUMBERS		
Media Type	Part Number	ISBN
USB	CFP1434A-USB	978-1-4799-2062-4

A wireless energy transceiver based on induction heating equipment

Stanimir Valtchev, Rui Neves-Medeiros
Department of Electrical Engineering, UNINOVA
Nova University of Lisbon
Caparica, Portugal
ssv@fct.unl.pt

Anastassia Krusteva, George Gigov, Plamen Avramov
Research and Development Sector
Technical University of Sofia
Sofia, Bulgaria
krusteva@tu-sofia.bg

***Abstract*—A contactless energy transmitter/receiver set is designed and its electrical parameters are tested varying the working frequency in the kHz range and the transceiver's distance. The goal is to improve the efficiency of the wireless charging of different batteries from the smart grid, guaranteeing more acceptable use of the electric vehicles.**

Keywords—wireless; energy; induction heating; transmitter; contactless; power; converter; smart grids; battery; electric vehicles

I. INTRODUCTION

Wireless On-Line Electric Vehicle Energy Transfer (WOLEVET) is a user-project within the Seventh Framework Programme (FP7) project Distributed Energy Resources Research Infrastructures (DERri) focused on battery charging when Wireless Energy Transfer (WET) is included. A bi-directional exchange of energy is planned between the AC grid, the battery and the contactless energy converter. The wireless energy transfer is defined as "On-line" because of the varying position of the energy receiver in relation to the energy transmitter. To experiment this movement the energy receiver was displaced at different distances to the fixed charging station. The described experiments were aimed to prove the most efficient energy transfer conditions that will facilitate the integration of electric vehicles (EV) in micro-grids, adding storage capacity (EV batteries) to the grid. This integration will reduce the battery size as the necessary energy will be directly available from the nearby source of the grid. This is very important as the price of a propulsion battery is now roughly 80% of the EV price. Smaller battery capacity means a fewer number of cells and hence lower environment pollution.

The WOLEVET project included the design and experimentation of two prototypes of contactless energy transmitter/receiver sets involving some available high frequency (HF) generators, most of them originally dedicated to induction and dielectric heating. One of the sets was built with "FLUXTROL 50" type ferrite plates and water cooled copper tubes and the other set, which is the subject of this work, was built with EE6527 ferrite plates and air cooled large section litz wire. The shape and the construction of the inductors that guarantee a good magnetic coupling and best efficiency are presented. The magnetic coupling is tested at active power of one or more kW. The important choice of the power inverter parameters is limited by the type of resonance and the switching frequencies of the already existing inverters.

After the introduction, the Chapter 2 explains the problem to be solved referencing the previous works. Chapter 3 intends to establish a mathematical relation between the circuit characteristics and the resulting mutual inductance. Experimental achievements are revealed in Chapter 4 and followed by some conclusions in Chapter 5.

II. STATE-OF-THE-ART

The EV and the hybrid electric vehicles (HEV) are already an urgent necessity due to environmental problems and growing prices of classical energy production. The available batteries, due to their specific energy capacity, will obligate the new vehicles to require a large number of charging cycles in different places and moments [1]. The resonant WET became vital, not only from the technical point of view, facilitating higher power transfer and increasing security, but also from the economical point of view, presenting itself as an easier, faster, cleaner and hence, more appealing solution for the daily user. As referred in [2], the unit sales of wireless EV chargers in North America will reach about 10,000 in 2014 and increase to more than 132,000 units by the end of the decade.

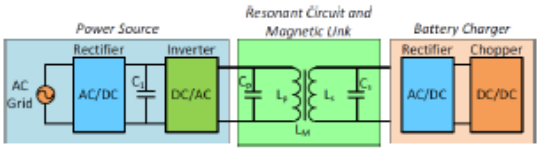

Fig. 1. Simplified WET system (based on [4]).

Fig.1 illustrates the operation of a simplified WET system. This functioning of the system is also reported in [3], [4] and [5]. The circuit action may be presented by the following blocks: the AC supply voltage is rectified and converted (in the charging station) to a high frequency AC pulses or other AC waveforms (usually sinusoidal or almost sinusoidal AC voltage at a frequency of several tens or hundreds of kHz). Based on the resonant processes this high frequency (electromagnetic or mainly magnetic) power is transferred to the EV side by induction. Finally the receiver converts the

high frequency AC power into a DC power for the battery charging.

The described process is in fact, very similar to the induction heating one. It is possible to see, by comparing Fig.1 and Fig.2 that the first two blocks of the systems are very alike. In the same time, instead of using the high frequency AC to inductively transfer electric energy, the electromagnetic excitation is applied to heat inductively the kitchen utensil closely positioned to the inductor, exhibited in Fig.2a and Fig.2b (article [6] refers to a domestic pan-inductor pair).

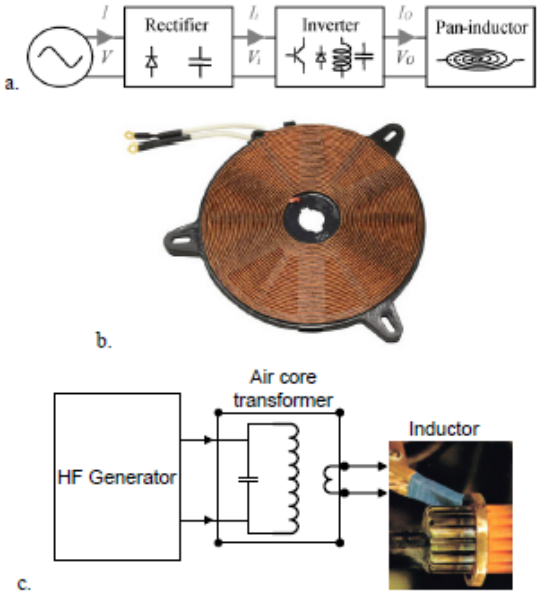

Fig. 2. Induction heating systems: a. Simplified domestic cooker [6]; b. Cooker inductor photo; c. Industrial High-Frequency (HF) heating equipment with HF transformer.

In the industry, as shown in Fig. 2c, for the purpose of intensifying the inductive heating in specific zones, the magnetic field is concentrated by water-cooled "inductors" conducting very high currents in a reduced number of turns, as mentioned in [7]. This operation (and the high voltage output of the HF generator require a current transformer constructed on air core. This "usual" inductive heating connection provokes difficulties in applying directly the high-power induction heating equipment to transfer DC power to the receiver side. For the experiments some of the original air core transformers were left attached as a matching circuit.

The inductively coupled power transfer for DC battery charging is based on the same principle of electromagnetic induction at high frequency. It is shown that the on-board receiver and the ground based transmitter of the charging station in Fig.3 transfer the AC (High-Frequency) energy to the electric vehicle (EV) through inductive transfer of energy, i.e. magnetic induction coupling. The only essential difference is the rectification and regulation process on the receiver side.

Many (all of them resonant) configurations are implemented in different wireless energy transfer constructions. The study of the Series Loaded Series Resonant (SLSR) converter places it as (maybe) the most suitable for the contactless energy transfer [8]. There are other possible resonant configurations as described in [9], equally capable to transfer energy and some of them quite effectively applied already.

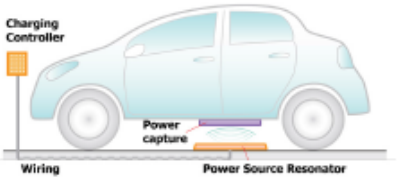

Fig. 3. Automotive wireless electric-energy transfer [2].

The SLSR power converter is becoming again popular after it appeared in the late 60-s and early 70-s in [10]. This happened first because of its Zero Voltage Switching (ZVS) characteristics and now it happens because of the growing necessity for contactless power transfer applications. The operation of SLSR converter is analyzed in many articles, e.g. in [8] but the obtaining of a rapid and accurate reaction of this circuit continues to be a problem. The existence of stored energy in the resonant reactance elements (inductance and capacitance) makes the direct control of the power switches quite difficult, especially when the circuit elements are not ideal and is not possible to be idealized (as is the case with WET).

Many articles are published, aimed at resonant converters control, usually including calculation of normalized phase-plane trajectory as in [11]. A more complex calculation block (implemented as FPGA) is shown in [12]. A computer model, developed in Korea Railroad Research Institute is presented in [13]. It is based on the so called "Valtchev model". Another control method that contemplates relatively large air gap is explained in [14].

All the known methods are not reacting immediately to the demand of the resonant tank as they measure and control the resonant current. The future Instant Energy Control (IEC) circuits that respond not so much to the resonant current but more to the resonant capacitor voltage are presented in [1] and [15]. This method of control gives a good perspective to the application of the SLSR converters, applying their current-source output characteristics and their good zero-voltage switching (ZVS) behavior. The IEC allows safer operation of the transmitter, but there is a lot to do for the future bi-directional energy transfer. Although the bi-directional transfer is not explicitly necessary, it will be a must for the future smart grids when the EV on the road will be included. In that case the charged vehicle is supposed to give back energy to the common grid (when necessary). The control of the bi-directional energy exchange is expected to be similar to the already known solutions but will be necessary to involve a new information grid, comparable to the mobile communications network although it seems to be necessarily

much faster. One of the main desirable functions will be to identify and authorize the car (e.g. that in Fig.3), efficiently and rapidly enough, to receive or to deliver energy passing near the transmitter cells and to continue this interchange with the next cell.

The US company Evatran, which is targeting home users, announced charging devices compatible with both Nissan Leaf BEV and Chevrolet Volt PHEV and converters adaptable for the Tesla Roadster and older Toyota RAV4 electric vehicles. The company installed its Plugless Power unit at Google's headquarters, where low-speed EVs are used to take workers and visitors around. Meanwhile, the WiTricity Corp. based in Watertown, Massachusetts, is banking on its relationships with larger companies (and MIT of course) to take a leadership position in the industry. The company last year started working with Delphi Automotive, General Motors´ former automobile parts division, on developing a wireless electric-vehicle charging system that uses magnetic resonance between a floor-mounted charging source and a vehicle. The possible positioning of the chargers in public and private places is shown in Fig.3 and Fig.4.

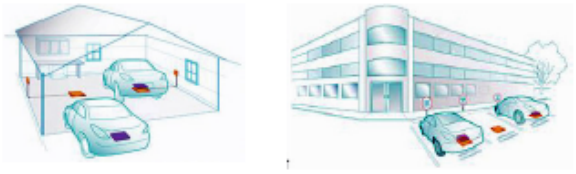

Fig. 4. Differently mounted wireless chargers [2].

A solution for the inductive charger of a bus implemented in Daejeon, Republic of South Korea, is shown in Fig.5. This version is different from the stationary charger as it uses many transmitters on the road in order to obtain an "on-line" charging, i.e. during the movement of the vehicle.

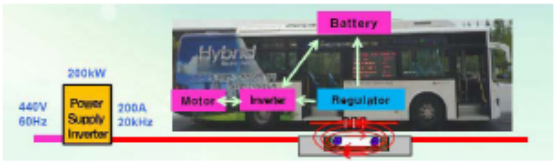

Fig. 5. The KAIST charging station. 440 V, 3 phase line [16], [17].

A soft-switching parallel converter is used for this application because this kind of topology is not sensitive to the parasitic inductance of the connecting cables between the high-frequency generator and the transmitting windings.

Although the connected by wires charger has a lot of definitive advantages such as simplicity and high efficiency, the inductive charger is safer, flexible and easy to use under any weather conditions ([16], [17]). The main drawbacks of the contactless charger are the high investment cost and the inevitable higher losses.

III. MUTUAL INDUCTANCE OF CIRCULAR COILS

It is important to understand how the mutual inductance will be affected by the dimensions of the coils. Although the planar elliptical shape of the transformer was the chosen one for the project, it is believed that the following equations, deduced from [18] for circular coils will provide sufficiently accurate results.

Mutual inductance is given by the expressions 7-34 and 7-36 from [18]:

$$M = \frac{\mu_0}{4\pi} N^2 d\phi \tag{1}$$

"N" represents the number of turns and the diameter is represented by "d".

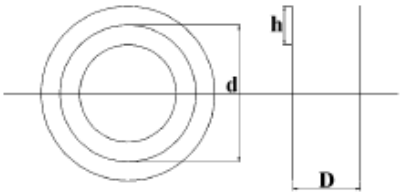

Fig. 6. Sketch of two circular coils.

The design on the left side in Fig.6 shows the considered average interior diameter. The drawing on the right side demonstrates the height "h" of the coils and the distance "D" between the two coils in magnetic coupling. Some parameters are used as normalized variables in (2) and (3).

$$\rho = \frac{h}{d} \tag{2}$$

$$\xi = \frac{D}{d} \tag{3}$$

$$\phi = \pi \left[\begin{array}{l} \left(1+\frac{3}{4}\xi^2+\frac{\rho^2}{24}-\frac{15}{64}\xi^4+\frac{7}{64}\xi^2\rho^2+\frac{11}{2880}\rho^4\ldots\right)\times \\ \times \ln\frac{16}{\xi^2+\rho^2}+\left(1+\frac{5}{8}\xi^2-\frac{161}{576}\xi^4+\frac{5}{8}\xi^2\rho^2\ldots\right)\times \\ \times\frac{\xi^2}{\rho^2}\ln\frac{\xi^2+\rho^2}{\xi^2}-4\left(1+\frac{2}{3}\xi^2-\frac{2}{5}\xi^4+\frac{2}{9}\xi^2\rho^2\ldots\right)\times \\ \times\frac{\xi}{\rho}arctg\frac{\rho}{\xi}-1+\frac{37}{24}\xi^2+\frac{43}{144}\rho^2-\frac{301}{360}\xi^4- \\ -\frac{\xi^2\rho^2}{720}+\frac{\rho^4}{75}+\ldots \end{array} \right] \tag{4}$$

To approximate the circular shaped coil formulas to the elliptical shape described in the Experimental results chapter, the following values were used:

$$h = 50mm\,;\ d = 140mm\,;\ D = 50mm\,;\ N = 5\,.$$

Therefore, the following parameters, necessary for the calculation in (4) were prepared:

$$\xi^2 = 0{,}128; \qquad \xi^4 = 0{,}0163$$

$$\rho^2 = 0{,}128; \qquad \rho^4 = 0{,}0163$$

$$\ln\frac{16}{\xi^2+\rho^2} = 4{,}135; \qquad \frac{\xi^2}{\rho^2} = 1$$

$$\ln\frac{\xi^2+\rho^2}{\xi^2} = 0{,}693; \quad arctg\frac{\rho}{\xi} = 0{,}785$$

$$\phi = 3{,}623$$

The mutual inductance, as a consequence of (1), results in:

$$M = 1{,}268\,\mu H$$

IV. Experimental Results

The main performed tasks were aimed to verify the efficient operation of the inductively coupled set of windings, together with their corresponding magnetic core, further designated as transmitter and receiver. This included the practical design and construction of the transmitter and the receiver (at this stage, identical), the proper choice of the resonant capacitor, the definition of the power for the experiments, the reconfiguration of the existing (from induction heating) system of coupling, the necessary measurements and analyses of the obtained parameters.

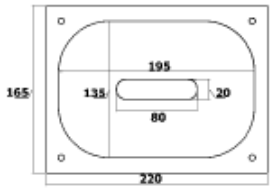

Fig. 7. Trasmitter/receiver design with dimensions in mm.

The designed transmitter (or receiver), illustrated in Fig.7 consists in ferrite core (EE6527 - CF139) and coils of litz wire with number of turns N = 5 and air cooling. The thickness of the plate is 15 mm and the internal column is 9 mm thick. The parameters of the coil are: L = 10,88 µH and R = 23,0 mΩ with the ferrite core and L = 4,16 µH and R = 43,6 mΩ without the core.

Four different experiments were attempted with four different power sources.

In this text the indexes "$_1$" and "$_2$" correspond respectively to the primary and the secondary sides of the transformer (named together "magnetic link" or "transceiver"). The primary side of the transformer will be also referred as "the sender" or "the first coil" and the secondary side as "the receiver" or "the second coil".

The index "$_r$" represents resonance.

The upper case "R" and "D" correspond to electrical Resistance and Distance respectively. Lower case "r" and "d" correspond to radius and diameter.

A. First experiment – Laboratory HF signal generator

Fig. 8. Transceiver with EE6527 ferrite and compensating capacitors

This experiment was aimed to determine the resonant frequency of the transceiver at low power. The circuit main parameters, such as voltages, currents and phases in primary and secondary sides, were simultaneously measured.

Both first and second coils are compensated by capacitors $C_1 = C_2 = 0{,}2$ µF (Fig.8). The experiments were realized at different distances from 5 to 20 cm, with the resistive load R_{load} = 54 Ω, maintaining the resonant frequency of the secondary circuit as the most important reference.

The measured and calculated parameters together with the efficiency are presented in Table I and in Table II.

TABLE I Measured Parameters for the Primary Side

D [cm]	f_1 [kHz]	U_1 [Vrms]	I_1 [mArms]	φ_1 [°]
5	118,23	1,44	27,30	
10	100,94	3,69	19,90	26.53
15	102,96	4,95	12,60	32.6
20	102,92	5,22	13,10	40.4

TABLE II. Measured and Calculated Parameters

D [cm]	U_2 [Vrms]	I_2 [mArms]	P_1 [mW]	P_2 [mW]	η [%]
5	1,30	16,60			
10	1,94	26,00	73.43	50.44	68.7
15	1,31	18,60	49.74	24.37	48.9
20	0,75	11,40	61.43	8.56	13.9

Some part of the oscilloscope images obtained in the first series of experiments is presented in Fig.9, Fig.10 and Fig.11. The blue lines represent voltage waveforms and the red lines represent current waveforms.

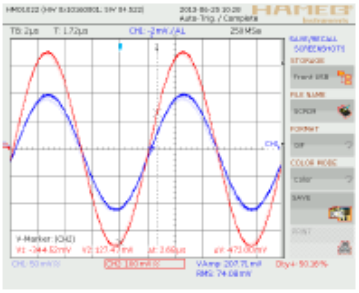

Fig. 9. Voltages U_2 and currents I_2 for distance D = 10 cm.

In Fig.9 it is possible to draw the conclusion that the voltage and the current in the secondary side of the transceiver for the distance of D = 10 cm are in phase, i.e. the resonance is obtained in the secondary.

Fig.10 and Fig.11 reveal an abnormal distortion affecting the current wave form. The growing distance aggravates that distortion. This atypical behaviour is justified by the predictable generator limitations, as the worst condition for the laboratory generator is observed when the load does not exist (the load is far away and the primary operates in short-circuit mode, receiving and delivering the same portions of energy from the input power supply).

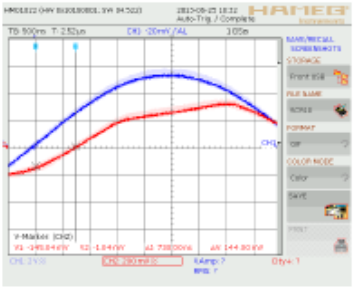

Fig. 10. Voltages U_1 and currents I_1 for distance D = 10 cm.

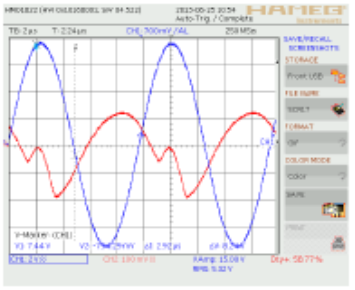

Fig. 11. Voltages U_1 and currents I_1 for distance D = 20 cm.

B. Second experiment - HF vacuum tube generator

The power for this experiment was much higher. The HF vacuum tube generator is prepared for industrial high power HF heating (Fig.12). Internally it has a transformer with a primary (vacuum tube output stage winding) and secondary (winding that is connected to the heating inductor, as shown in Fig.2). The primary coil (the transmitter) is now replacing the induction heating inductor and it is connected in parallel to the secondary side of the HF generator output transformer. This is not the best connection for obtaining the highest efficiency, but in this way the generator schematic changes are kept to the minimum and it is easy to reconfigure it again for inductive heating purposes. The high power generator is visible in Fig.12 in the background of the photo.

Fig. 12. Magnetic cores of the coils, shaped as two identical planar ferromagnetic EE6527 plates.

The primary compensating capacitor has a capacitance C_1= 5000 pF. The secondary coil of the transceiver (it is the receiver if the energy flux is unidirectional, as in this case) has in parallel a compensating capacitor of C_2=6800 pF. The switching frequency is f = 538 kHz, applying the calculated secondary inductance of the receiver L_2 = 12,8 µH. In this photo (Fig.12) as a load to the transceiver (its receiver side) is connected an incandescent lamp of 100W, i.e. R_{load} = 45 Ω. Experiments are made for different distances between the two coils: D = 12 cm, D = 18 cm and D = 24 cm. Two values are used as supply voltage in the generator anode: Ua = 1500 V and Ua = 2100 V.

The experimental results and the values calculated, based on those results, for D = 18 cm, are presented in Table III and in Table IV.

TABLE III. RESULTS FOR D = 18 CM AND A FREQUENCY OF OPERATION F = 538 KHZ (A)

Ua [V]	U_1max [V]	I_1max [A]	φ_1 [°]	P_1 [W]
1500	240	1,14	58o	72.49
2100	320	1,53	58o	129.49

TABLE IV. RESULTS FOR D = 18 CM AND OPERATION FREQUENCY F = 538 KHZ (B)

Ua [V]	U_2max [V]	I_2max [A]	P_2 [W]	η [%]
1500	90	0,85	38,25	52.7
2100	140	1.14	79,8	61.6

Primary and secondary voltages are measured also for D = 12 cm and D = 24 cm and shown in Table V:

TABLE V. PRIMARY AND SECONDARY VOLTAGES

Ua [V]	D [cm]	U_1max [V]	U_2max [V]
1500	12	280	200
2100	24	280	70

The data concerning the anode voltage in this case show that the generator here is a vacuum tube type, which is still the most widely used generator for the frequency range of 400-500 kHz. The induction heating and melting of highly conductive, non-ferromagnetic details requires that frequency. To regulate the power it is a common practice to regulate the anode supply voltage of the vacuum tubes.

C. *Third experiment - MOSFET, phase shift regulated and full bridge inverter*

The power converter used in this experiment was prepared for several (more than 5) kW. The compensation is made by $C_1 = C_2 = 0,2$ µF, the experimented distance is D = 10 cm, D = 15 cm, or D = 20 cm. The load was varied between 2,5 and 11,5 Ω.

TABLE VI. PARAMETERS OF THE INVERTER MEASURED IN THE PRIMARY SIDE OF THE TRANSMITTER

D [cm]	f [kHz]	U_1 [Vmax]	I_1 [Amax]	φ_1 [°]	P_1 [W]
10	130,1	600	36	85,3	885
	130,0	600	31,25	85,3	775
	130,0	600	30	85,3	737
15	151,7	600	33,6	85,3	826
	130,0	600	31,25	85,3	768
20	130,0	600	30	88,8	184

The obtained parameters for the primary side of the transceiver are presented in Table VI. For the secondary side of the transmitter, the values of the electric parameters and the efficiency are presented in Table VII. The rectifier circuits in this case were not applied, because of the batteries that were not properly prepared. The active power in the secondary is the main parameter for the circuit comparison. The active power is the parameter that is required for the inductive heating too.

TABLE VII. PARAMETERS OF THE SECONDARY SIDE OF THE TRANSMITTER AND CALCULATED EFFICIENCY

D [cm]	Rload [Ω]	U_2 [Vmax]	I_2 [Amax]	φ_2 [°]	P_2 [W]	η [%]
10	2,5	112,14	8,16	30,4	395	44,6
	11,5	130,14	5,22	21,1	317	40,9
	2,5	100,14	7,5	28,0	332	45,0
15	2,5	90	7	31,5	269	32,5
	11,5	113,65	4,98	22,5	261	34,0
20	2,5	24,02	5,43	45,3	46	25,0

A part of the oscilloscope images obtained in the third experiment is presented in Fig.13, Fig.14 and Fig.15.

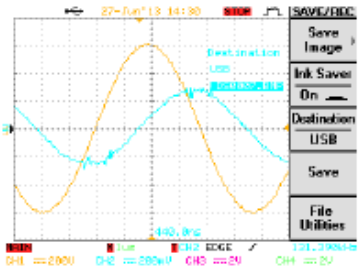

Fig. 13. Voltage U_1 and current I_1 for D = 10 cm and R_{load} = 2,5 Ω.

Fig.13 demonstrates the phase shift between the primary voltage and the primary current for the case D = 10 cm and R_{load} = 2,5 Ω. Even without measurements it can be eye witnessed that the phase shift is too high. In this case its value is around φ = 85°. Consequently the power drops considerably.

Fig.14 and Fig.15 together are useful to deduce the phase shift between the secondary voltage and the secondary current. For the case D = 10 cm and R_{load} = 2,5 Ω, the phase shift is φ = 30°.

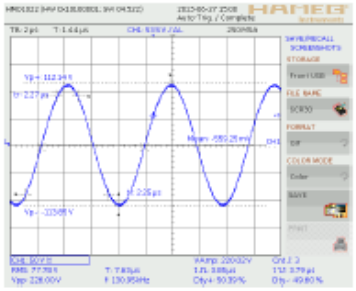

Fig. 14. Voltage U_2 for D = 10 cm and R_{load} = 2,5 Ω.

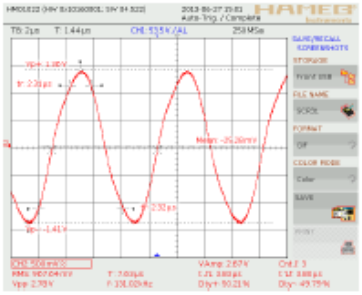

Fig. 15. Current I_2 for D = 10 cm and R_{load} = 2,5 Ω.

Conclusions

The comparative analysis of the experimental results reveals the complexity of the problems and results in the following conclusions: the efficiency is related to the frequency and at the same frequency it is related to the load. The highest obtained output voltage depends on the input voltage and the distance transmitter/receiver. For these generators a cooling was needed at the highest transferred power.

Several measurements were acquired with different distances from 5 to 20 cm. For the transceiver based on EE6527 ferrite plates and air cooled litz wire, the highest efficiency value was nearly 70% with a correspondent distance of 10 cm. All the experiments were hold at almost the same HF generator schematics, as it was originally projected. In the future, by applying a dedicated construction, the efficiency will be higher.

In conclusion, the experiments have proven that the existing induction heating equipment (and the knowledge accumulated in the inductive heating laboratories) can be used as a base for developing the new WET technology, especially for charging the batteries of the EV. It is a faster solution of the future problem and it can guarantee a better cooperation between the electric vehicles and the grid.

Acknowledgments

The authors fully recognize the support from the European Commission FP7 project DERri GA No 228449 (http://www.der-ri.net). The authors are entirely responsible for the content of this publication. It does not represent the opinion of the European Community. We thank equally the enterprise Apronecs (Bulgaria) that allowed us to experiment at higher power levels. We thank also the research organization UNINOVA from Universidade Nova de Lisboa (Portugal) for the support to the paper presentation.

References

[1] P. Van den Bossche, F. Vergels, J. Van Mierlo, J. Matheys, W. Van Autenboer, "SUBAT: An assessment of sustainable battery technology", Journal of Power Sources, vol. 162, no. 2, pp. 913–919, November 2006.

[2] AutoObserver, "Siemens enters fragmented wireless charging market": http://www.autoobserver.com/2011/04/siemens-enters-fragmented-wireless-charging-market.html.

[3] P. Bauer, "Contactless power transfer: inductive charging of EV": http://www.d-incert.nl/wp-content/uploads/2010/12/Pavol-Bauer-Groningen-Presentatie.pdf.

[4] A. Neves, D. M. Sousa, A. Roque, J. M. Terras, "Analysis of an inductive charging system for a commercial electric vehicle", European Conference on Power Electronics and Applications, pp. 1–10, Birmingham, August/September 2011.

[5] Qualcomm Halo Video: http://www.youtube.com/watch?feature=player_embedded&v=ksCgpqMgcZI.

[6] J. M. Burdío, F. Monterde, J. R. García, L. A. Barragán, A. Martínez, "A two-output series-resonant inverter for induction-heating cooking appliances", IEEE Transactions on Power Electronics, vol. 20, no. 4, pp. 815–822, July 2005.

[7] A.C. Metaxas, Foundations of Electroheat - A Unified Approach, Chichester, England, John Wiley & Sons Ltd, 1996.

[8] S. Valtchev, J. B. Klaassens, "Efficient resonant power conversion", IEEE Transactions on Industrial Electronics, vol. 37, no. 6, pp. 490–495, December 1990.

[9] C. S. Wang, O. H. Stielau, G. A. Covic, "Design considerations for a contactless electric vehicle battery charger", IEEE Transactions on Industrial Electronics, vol. 52, no. 5, pp. 1308-1314, October 2005.

[10] F. C. Schwarz, "A method of resonant current pulse modulation for power converters", IEEE Transactions on Industrial Electronics and Control Instrumentation, vol. IECI-17, no. 3, pp. 209–221, May 1970.

[11] L. Rossetto, "A simple control technique for series resonant converters", IEEE Transactions on Power Electronics, vol. 11, no. 4, pp. 554–560, July 1996.

[12] A. Moradewicz, M. Kazmierkowski, "FPGA based control of series resonant converter for contactless power supply", IEEE International Symposium on Industrial Electronics, pp.245–250, Cambridge, June/July 2008.

[13] J. V. P. P. Dias, H. Kim, D. Jang, "Computer model for railway inductive power supply using Valtchev model", International Conference on Electrical Machines and Systems, pp. 1–6, Beijing, August 2011.

[14] F. van der Pijl, P. Bauer, M. Castilla, "Control method for wireless inductive energy transfer systems with relatively large air gap", IEEE Transactions on Industrial Electronics, vol. 60, no. 1, pp. 382–390, January 2013.

[15] S. Valtchev, K. Brandisky, B. Borges, J. B. Klaassens, "Resonant contactless energy transfer with improved efficiency", IEEE Transactions on Power Electronics, vol. 24, no. 3, pp. 685–699, March 2009.

[16] S. Lee, J. Huh, C. Park, N. Choi, G. Cho, C. Rim, "On-line electric vehicle using inductive power transfer system", Energy Conversion Congress and Exposition, pp. 1598–1601, Atlanta, September 2010.

[17] M. Park, E. Shin, H. Lee, I. Suh, "Dynamic model and control algorithm of HVAC system for OLEV® application", International Conference on Control Automation and Systems, pp. 1312–1317, Gyeonggi-do, October 2010.

[18] P. Kalantarov, L. Tseitlin, Calculation of inductances (in Rus: Расчёт индуктивностей), 3rd revised edition, Leningrad (St Petersburg), Russia, Ed. Energoatom, 1986, p. 308.